Catalysis Today 140 (2009) 127–134

Contents lists available at ScienceDirect

Catalysis Today

journal homepage: www.elsevier.com/locate/cattod

Fischer-Tropsch Synthesis Catalyst activation of low alpha iron catalyst

Mingsheng Luo [a], Hussein Hamdeh [b], Burtron H. Davis [a,*]

[a] Center for Applied Energy Research, 2540 Research Park Drive, Lexington, KY 40511, USA
[b] Physics Department, Wichita State University, Wichita, KS, USA

ARTICLE INFO

Article history:
Available online 22 November 2008

Keywords:
Iron catalyst
Fischer-Tropsch Synthesis
Catalyst activation
Iron carbides
Mössbauer spectroscopy
Potassium
Promotion
Pretreatment
Reduction
Activation
Syngas

ABSTRACT

Activation with three different gases (H_2, CO and synthesis gas) over an Fe100/K1.4/Si4.6/Cu2.0 catalyst was conducted to investigate the effects of pretreatment gas on Fischer-Tropsch Synthesis (FTS) activity and selectivity. Catalyst slurry was withdrawn from the reactor at increasing time intervals of FTS for Mössbauer spectroscopic analysis. Activation with CO produced the highest syngas conversion while H_2 generated the lowest; syngas activation produced a slightly lower conversion than CO activation. CO activation transformed the majority of the iron into χ-Fe_5C_2 and Magnetite with only 12% ε-$Fe_{2.2}C$ being detected. Unlike the CO activated catalyst, the syngas activated iron catalyst resulted in a lower amount of χ-Fe_5C_2 than ε-$Fe_{2.2}C$. The initial high (64%) content of ε-$Fe_{2.2}C$ decreased gradually to below 30% while CO conversion decreased from 83% to 55%. During this period, χ-Fe_5C_2 increased from initial 10% to 33%. Magnetite changed little during the process while the form of carbides interchanged. Hydrogen activation yielded a low CO conversion of 50% and only 8% χ-Fe_5C_2 and 16% ε-$Fe_{2.2}C$ was formed while Magnetite was as high as 75% after the FTS reaction rate became constant. Although activation gas type had a significant effect on syngas conversion, hydrogen, syngas and CO activations produced similar H_2 to CO usage ratio, hydrocarbon product distribution, olefin fraction, alpha value and CO_2 selectivity.

1. Introduction

Hydrocarbons are produced from CO and H_2 by the Fischer-Tropsch Synthesis (FTS):

$$(2n+1)H_2 + nCO \rightarrow C_nH_{2n+2} + nH_2O \quad (1)$$

Cobalt and iron are today the only feasible commercial catalysts for an FTS process. When an iron catalyst is used for FTS, the water–gas shift (WGS) reaction can also occur. This reaction consumes CO and water formed by the FTS reaction to produce additional hydrogen as well as carbon dioxide.

$$H_2O + CO \leftrightarrow CO_2 + H_2 \quad (2)$$

This WGS activity makes the iron catalyst a better choice in a coal-based FTS. As the world crude oil price continues to increase, FTS becomes a feasible alternative to petroleum. In a typical iron catalyst, silica, copper and potassium are added to improve the properties of the catalyst. Copper is added to aid in the reduction of iron [1–4], and silica is a structural promoter added to stabilize the surface area [1,3,5]. Silica may also have a chemical effect on the catalyst properties [3,6–8]. Potassium is considered to promote CO dissociation and enhance chain growth [1–3,5,9–11]. It increases both the FT activity and the olefin yield, but lowers the CH_4 fraction [12–14]. Potassium can also increase the catalytic activity for FTS and water–gas shift reactions [2,13,15–18].

Pretreatment of iron catalysts has an important influence on the FTS activity and selectivity [19]. A cobalt catalyst is usually activated with H_2 and metallic cobalt is believed to be the active phase for FTS; however, the iron catalyst system is not as simple as that of a cobalt catalyst. Anderson pointed out that without pretreatment the iron catalyst is inactive, and that H_2, CO, or H_2 + CO can reduce the catalyst at 200–300 °C [20]. He found that at 0.01 MPa and 325 °C, pure CO was a better reduction gas than syngas ($1H_2$ + 1.5CO). Based on a 50% gas contraction ratio (not including CO_2), a catalyst following CO pretreatment was reported to maintain a service life for 350 days while a syngas pretreated material has a life of only 200 days. Carbides are probably the active phase for FTS, even with H_2 activation. Metallic iron is reported to rapidly transform to Hägg carbide (Fe_5C_2) upon introducing syngas [12]. Further reducing and carbiding continues for several days so that the activity will show an initial conditioning period. During this period, the surface area decreases

* Corresponding author. Tel.: +1 859 257 0253; fax: +1 859 257 0302.
E-mail address: davis@caer.uky.edu (B.H. Davis).

0920-5861/$ – see front matter © 2008 Elsevier B.V. All rights reserved.
doi:10.1016/j.cattod.2008.10.004

and the pore diameter increases. Shroff et al. [21] claimed neither Hematite nor Magnetite have FT activity.

Reduction of an iron catalyst (α-Fe_2O_3) with hydrogen proceeds via Magnetite (Fe_3O_4) and presumably Woestite (FeO) to metallic iron [22,23]. Because Woestite is metastable below 843 K (573 °C) [22–24] and any FeO is quickly transformed to Fe_3O_4 and Fe, the formation of FeO is hardly observed. Reduction of Fe_3O_4 with H_2 to zero valence was also claimed [25–27], with 20% metallic iron being obtained by treating with H_2 at 220 °C.

Baltrus et al. [28] applied XPS, Auger spectroscopy and ion spectrometry to study the state of surface Fe and carbon and the distribution of K and Cu over the surface of a Fe/K/Cu catalyst. They found that the surface K/Fe ratio following CO + H_2 reduction was greater than that from CO reduction; therefore, they indicate that a CO + H_2 reduction resulted in a more inactive carbon deposit which covered part of the active carbide surface.

Sudsakorn et al. [29] studied a 100Fe/5Cu/4.2K/11SiO_2 iron FT catalyst in a 4 mm microreactor. XRD data indicate that H_2 activation transferors Fe phases to FeO + Fe_3O_4, and to Fe carbides + Fe_3O_4 for both CO and syngas activation. Sault [30] studied the activation effect of CO or H_2 on Fe/K/Cu = 100/0.2/3 (wt%) and Fe/K/Cu/Si = 100/4.2/5/25 catalysts using Auger Electron Spectroscopy. They found that CO conversion over a Fe/K/Cu = 100/0.2/3 (wt%) catalyst can vary by a factor of nearly three, depending on the activation conditions. H_2 activation leads to the rapid transformation of Fe_2O_3 to metallic iron and segregation of sulfur to the surface [30]. Sulfur arises from bulk sulfate impurities present from the catalyst preparation. Sulfur coverage increased with activation time and temperature since the sulfur diffusion rate increases as the temperature increases. CO conversion over a Fe/K/Cu/Si = 100/4.2/5/25 catalyst changed to a much lesser extend with activation conditions. No significant surface composition change was observed over the iron catalyst with a higher K content. They believed that this result was due to the difference in surface area and the reducibility of the two catalysts.

Pretreatment of an iron catalyst with CO or syngas can result in the formation of χ-carbide [31–34]. Bukur et al. [27] studied the activation effect on K/Fe = 0.8/100 (wt%) catalyst in a fixed bed reactor and concluded that CO activation at 280 °C led to higher initial FTS activity and a higher fraction of long chain hydrocarbons than an H_2 activated catalyst. Bian et al. [35] used a precipitated Fe_2O_3 catalyst precursor that was reduced by H_2 or CO and characterized the catalysts using diffuse reflectance FT-IR (DRIFT) with high-pressure syngas adsorption, syngas temperature-programmed desorption (TPD), XRD and BET surface area. Their results show that for the H_2-reduced sample metallic iron particles are formed and on the CO-reduced sample a mixture of metallic iron and iron carbides are formed. The iron carbides on the CO-reduced sample can be decomposed to metallic iron by H_2 treatment at 300 °C, and the metallic iron on the H_2-reduced sample can be partly converted to iron carbides by CO treatment at 300 °C. Both the metallic iron and iron carbides on the reduced samples have high activity for CO dissociation.

Mössbauer spectroscopy is an effective way to analyze iron catalysts. In situ Mössbauer studies have been reported [36,37], but only for cases where the samples were produced at low conversion and pressure. Other studies at commercial conditions were conducted by removing a sample from the reactor followed by a careful passivation [38]. This process, if not performed properly, allows the sample to oxidize; thus, handling of the catalyst sample is crucial to obtain reliable result for iron catalysts [21]. At low to moderate FTS reaction conditions (<270 °C), only ε-$Fe_{2.2}C$ and χ-Fe_5C_2 were formed [27,39], while θ-Fe_3C was reported only for high temperature FT synthesis with fused iron catalysts [12]. After activation, Magnetite (Fe_3O_4) is also found in the iron FT catalysts and Magnetite has been reported to be both active [23] and inactive for FT synthesis [20]. This discrepancy may be a result of improper handling of the used catalyst samples for Mössbauer spectroscopy [40,41]. Some researchers suggested that ε-carbide and ε'-carbide are responsible for the catalysis following CO dissociation [42,43]. Some claim that Hägg carbide has a low activity [36,44]. On the other hand, some claim that deactivation of iron FT catalysts is associated with the transformation of Hägg carbide to a less active ε-carbide phase with the formation of highly ordered graphite on the catalyst surface [44].

A direct relation of carbide formation and syngas conversion was reported by Amelse et al. [45] and by Raupp and Delgass [46]. Calcined and reduced 5 wt% Fe/SiO_2 catalysts were found to be completely carbided by the FTS reaction mixture (syngas). The stability of different carbides was reported to be in the decreasing order of ε'-$Fe_{2.2}C$ < ε-Fe_2C < χ-Fe_5C_2 < θ-Fe_3C. While χ-Fe_5C_2 was reported to be characteristic of unpromoted fused or precipitated iron catalysts, ε-Fe_2C was the phase reported for K_2O and/or Cu promoted catalysts [47]. The stable θ-Fe_3C can be formed only at above 750 K [46]. Silica had a stabilizing effect on ε-Fe_2C because this phase is stable only below 490 K, and can be converted to χ-Fe_5C_2 at 493–673 K [45]. The stabilization effect of silica depends on the particle size. Raupp and Delgass [46] studied FTS at 250 °C on 20 wt% Fe/SiO_2 catalyst and they found that for small particles (d = 6–7 nm), the less stable ε'-$Fe_{2.2}C$ and ε-Fe_2C are formed, similar to the results by Amelse at el. [45]. On large particles (d = 10 nm) the more stable χ-Fe_5C_2 is formed during the carburization process.

Studies with ^{13}C tracers showed that carbon on the surface of carbided catalysts is incorporated to a small extent in FT products [48]. The influence of activation gas and conditions on FTS activity and selectivity over iron catalysts was investigated in our previous work [49–51]. In this study, we have compared the rate and conversion products of typical low alpha iron catalysts together with the phases of iron present in the catalyst at various times on stream.

2. Experimental

2.1. Preparation of catalyst

Precipitated iron catalysts were prepared using a ferric nitrate solution obtained by dissolving $Fe(NO_3)_3{\cdot}9H_2O$ in distilled and deionized water, and then tetraethylorthosilicate was added to provide the desired Fe:Si ratio. The mixture was stirred vigorously until the tetraethylorthosilicate had hydrolyzed. A flow of the tetraethylorthosilicate and iron nitrate mixture was added to a CSTR precipitation vessel together with a stream of 30% ammonium hydroxide that was added at a rate to maintain a pH of 9.0. By maintaining the slurry pH at 9.0 and an average residence time of 6 min, a base catalyst material containing iron and silicon was obtained. The slurry from the CSTR was filtered with a vacuum drum filter and the solid was washed twice with deionized water. The final filter cake was dried for 24 h in an oven at 110 °C with flowing air. For this study, the Fe:Si catalyst base powder was then impregnated with the proper amount of aqueous K_2CO_3 and $Cu(NO_3)_2$ solution to produce the desired composition of Fe:Si:K:Cu = 100:4.6:1.44:2.0 (atomic ratio). The catalyst was dried at 110 °C overnight with good mixing followed by impregnation and calcination at 350 °C in an air flow for 4 h.

2.2. In situ activation of catalysts

In this study, the potassium promoted iron catalyst batches were pretreated with CO, syngas (H_2:CO = 0.7) or H_2 at 270 °C for

24 h. Carbon monoxide activation was carried out at 1.3 MPa. The CO flowed through a catalyst slurry containing 10% solids in 300 mL of Durasyn (a mixture of decene trimers). The reduction of Fe_2O_3 with CO is considered to occur in two steps:

$$3Fe_2O_3 + CO \rightarrow 2Fe_3O_4 + CO_2 \quad (3)$$

$$5Fe_3O_4 + 32CO \rightarrow 3Fe_5C_2 + 26CO_2 \quad (4)$$

In addition, CO_2 may be formed by the Boudouard reaction:

$$2CO \rightarrow C + CO_2 \quad (5)$$

Previous work in our laboratory showed that approximately 50–75% more carbon was present in the CO-activated catalyst mass than was needed to form Fe_5C_2 [32].

Activation of Fe_2O_3 with H_2 also occurs in two steps but with metallic iron as the final product:

$$3Fe_2O_3 + H_2 \rightarrow 2Fe_3O_4 + H_2O \quad (6)$$

$$Fe_3O_4 + 4H_2 \rightarrow 3Fe + 4H_2O$$

Our previous work indicated that high pressure had a detrimental effect on iron catalyst activity when hydrogen or syngas was used in activation process [49]; thus, atmospheric pressure was used in H_2 and syngas reductions in this study. A two-step reduction using H_2 and then CO was also investigated to test the synergism in comparison to the single step reductions. Table 1 shows the detailed conditions for iron catalyst reduction and FTS reactions.

2.3. Mössbauer analysis

Slurry samples were withdrawn from the reactor following activation and during increasing time intervals during the synthesis. A dip-tube extended to the bottom of the reactor to permit withdrawal of samples from the slurry in the reactor. Prior to collecting a sample, sufficient slurry was withdrawn to clean the withdrawal tube of prior sampling material and then about five grams of slurry were withdrawn from the reactor. The end of the outlet of the sampling tube was covered by a tent that was flushed with nitrogen to prevent the sample from contacting the air. The withdrawn sample would cool to become a solid within 2–5 min. The sample was stored in a glove box flushed with nitrogen prior to transferring a portion of the sample to the Mössbauer sample holder. The holder was closed and placed in a bottle that was flushed with xenon prior to closing it. The sample was shipped to Wichita, Kansas for analysis.

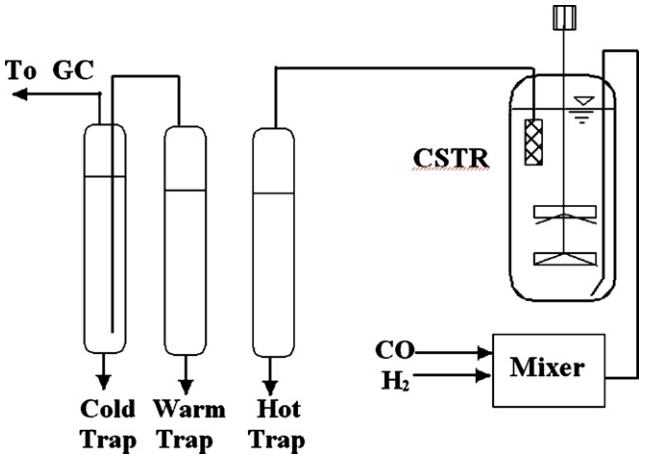

Fig. 1. CSTR Fischer-Tropsch Synthesis reactor system.

2.4. Reactor system

As shown in Fig. 1, a 1-l continuous stirred tank reactor (CSTR) was used in this study. A stainless steel mesh filter was installed to allow removal of wax samples from the catalyst slurry to be collected in a hot trap held at 200 °C. A warm trap (100 °C) and cold trap (0 °C) were used to collect liquid (mixture of liquid wax, oil and water) samples, by condensing from the vapor phase which was continuously withdrawn from the reactor vapor phase.

CO and H_2 mass flow controllers were used to provide a gas flow to yield a simulated synthesis gas of the desired composition. After the catalyst was activated, syngas was introduced at a rate of 5.0 SL/(h g-Fe). Reaction conditions were 270 °C, 1.3 MPa, H_2/CO = 0.7, and a stirrer speed of 750 rpm.

2.5. Product sampling and analysis

Daily gas, water, oil, light and heavy wax samples were collected and analyzed. Table 2 is a summary of the instruments

Table 1
Activation and FTS conditions.

Run ID	Activation			FTS		
	Gas type	Temp. (°C)	Pressure (MPa)	Temp. (°C)	Pressure (MPa)	Space velocity (SL/(h g-Fe))
C-136	CO	270	1.3	270	1.3	3.1
H-63	H_2	270	0.1	270	1.3	3.1
S-69	Syngas	270	0.1	270	1.3	3.1

Table 2
Instruments for analysis of FTS products.

Instrument	Sample	GC detector	GC conditions
HP Quad Series Micro GC	Gas	TCD	[a]
HP5790 GC	Water	TCD	6′ × 1/8″ SS packed column, Porpak Q, program from 100 °C at 8 °C/min to 245 °C, hold 8 min
Agilent 6890	Liquid oil	FID	DB5 column, 60 m length, 0320 mm ID, 0.25 μm film thickness, program, hold 10 min at 35 °C, ramp 4 °C/min to 325 °C, hold 40 min
Agilent 6890	Solid wax	FID	Aluminum clad HT5 column, 25 m length, 0.53 mm ID, 0.15 μm film thickness, program from 50 °C at 10 °C/min to 400 °C, hold 40 min

[a] Column 1: 10 m × 0.32 mm ID, 30 mn film molecular sieve 5A isothermal at 110 °C; Column 2: 8 m × 0.32 mm ID, 10 mm film, ParaPlotU isothermal at 80 °C; Column 3: 10 m × 0.32 mm ID, 8 mm film alumma isothermal at 140 °C; Column 4: 10 m × 0.15 mm ID, 2 μm film OV-1 isothermal at 120 °C.

used for gas, solid wax, liquid oil, and water analysis. The light wax and water mixture was collected daily from the warm trap and an oil plus water sample from the cold trap. Incondensable tail gas from the cold trap was analyzed with an online HP Quad Series Micro GC, providing molar compositions of C_1–C_4 olefins and paraffins as well as for H_2, CO and CO_2. Hydrogen and carbon monoxide conversions were calculated based on the GC analysis results and the gas flows entering and exiting the reactor, using the following formula (N = moles of gas):

$$\text{Conversion}\,(\%) = \left(\frac{N_{\text{in}} - N_{\text{out}}}{N_{\text{in}}}\right) \times 100 \tag{8}$$

The oil and light wax samples were mixed before analysis with an Agilent 6890 Series GC. The heavy wax was analyzed with an HP5890 Series II Plus GC while the water sample was analyzed using an HP5890 Series II GC.

3. Results and discussion

3.1. Activity

To investigate the effects of gas type and activation conditions on FTS activity and selectivity, activation with three different activation gases (i.e., H_2, CO and syngas) were conducted at 270 °C. Our previous work indicated that high pressure had a detrimental effect on iron catalyst activity when hydrogen was used in activation process [49]; thus an atmospheric pressure was used in H_2 and syngas reduction in this study. Table 1 shows the detailed conditions for high-alpha iron catalyst reduction and FTS reactions.

Table 3 gives the results of the FTS reactions using different activation gases after the FTS conversion was stable. In addition to the conversion (Eq. (8)), H_2 to CO usage was the ratio of H_2 reaction rate to CO reaction rate:

$$H_2/\text{CO usage} = \frac{r_{H_2}}{r_{\text{CO}}} \tag{9}$$

Methane and CO_2 selectivity were calculated as

$$\frac{\text{CH}_4(\text{or\_CO}_2)\text{Produced}}{\text{CO\_Consumed}} \times 100\% \tag{10}$$

Table 3
Low-alpha iron FTS catalyst activity and selectivity results.

Activation gas	CO	H_2	Syngas
Conversion (%)			
CO	86.2	53.4	78.7
H_2	76.9	47.9	69.5
Syngas	82.5	51.2	75.0
H_2 to CO usage	0.60	0.60	0.59
Hydrocarbon rate (g/(h g-iron))	0.56	0.34	0.49
Selectivity (%)			
CH_4	6.41	7.18	6.49
CO_2	45.6	47.1	47.5
Hydrocarbon fractions (wt%)			
C_{1-4}	38.6	30.9	36.0
C_{5-11}	35.9	43.1	37.1
C_{12-18}	12.4	15.1	13.9
C_{19+}	13.1	10.9	13.0
Olefin ratio (mol%)			
C_2	31.4	54.8	42.7
C_3	81.6	82.1	82.8
C_4	81.3	77.2	81.0

Olefin ratio is the molar ratio of olefins to total hydrocarbon products:

$$\text{Olefin ratio} = \frac{\text{Olefins}}{\text{Olefins} + \text{Paraffin}} \tag{11}$$

Among the three activations, CO produced the highest syngas conversion (82.5%) while H_2 generated the lowest (51.2%). Syngas activation produced a slightly lower conversion than CO. Although activation gas type had a significant effect on syngas conversion, H_2/CO usage ratio was not affected, producing similar values of ~0.6.

The data in Table 3 also show that the influence of activation gas on the hydrocarbon rate was similar to that for syngas conversion. The highest hydrocarbon rate was obtained from CO activation (0.56 g/(h g-Fe)), which was slightly higher than from syngas activation (0.49 g/(h g-Fe)). The lowest hydrocarbon production rate (0.34 g/(h g-Fe)) was produced from H_2 activation.

Fig. 2 is the Mössbauer spectrum obtained at 20 K from CO reduced iron catalyst after 143 h of FTS reaction. At this reaction time, the CO conversion had become stable after undergoing an initial conditioning period, which lasted approximately 70 h. It has been reported that CO activation transformed the majority of the iron into χ-Fe_5C_2 for a kaolin-containing catalyst [41]; a small amount of superparamagnetic carbide was not identified and this may be small particle ε-$Fe_{2.2}C$ [52]. Fig. 2 shows that χ-Fe_5C_2 is the major component of the iron phase; about 46% χ-Fe_5C_2, 12% ε-$Fe_{2.2}C$ and 44% Magnetite were present. It is shown in Fig. 3 that after CO activation, the high content of carbide parallels the high conversion. After the initial induction period, the total carbide accounts for over 60% of the phases and more than two thirds of the carbides are χ-Fe_5C_2.

When hydrogen was used in activation step, some of the iron was converted to metallic iron. Fig. 4 is the Mössbauer spectrum obtained at 20 K from an H_2 reduced iron catalyst after 143 h of FTS reaction. As shown in Fig. 5, a CO conversion of 50% was produced after 100 h of reaction time. The amounts of iron carbides are low compared to what was obtained with the CO activation. About 20% metallic iron was present at the end of the 24 h hydrogen reduction period and the start of the reaction (time 0). During the reaction induction period, part of the Magnetite was transformed to carbides before the amounts of both the carbides and Magnetite become essentially constant. At the stable 50% conversion level, only 8% χ-Fe_5C_2 and 16% ε-$Fe_{2.2}C$ were present, with about 75% of

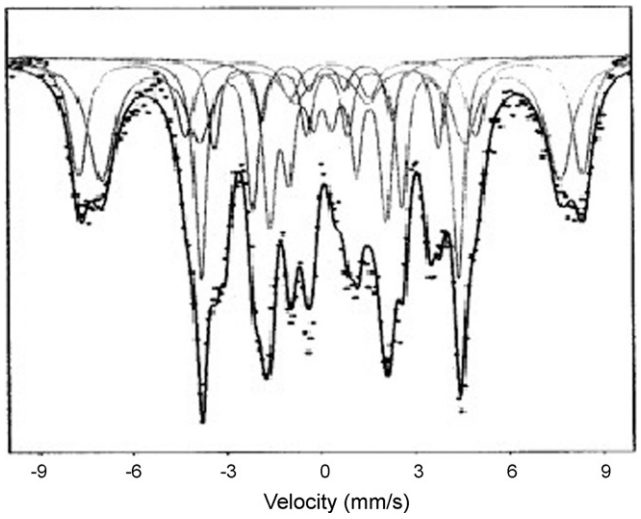

Fig. 2. Mössbauer spectrum at 20 K of catalyst after CO activation and 143 h reaction time. (Fe_3O_4, 42%; χ-carbide, 46%; ε-carbide, 12%).

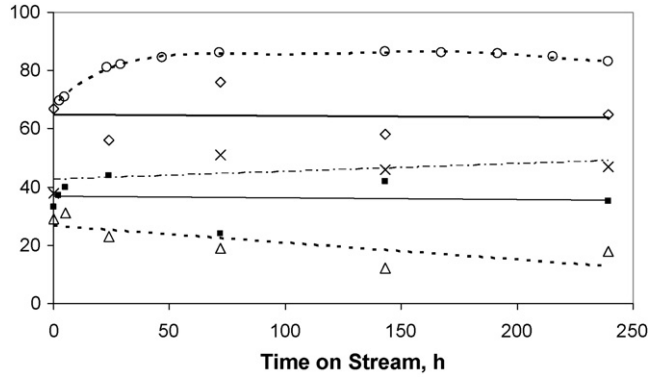

Fig. 3. CO conversion and iron carbide phases present for a CO activated iron catalyst and changes during synthesis (○, CO conversion; ■, Magnetite; △, ε-carbide; ×, χ-carbide; ◇, total carbides).

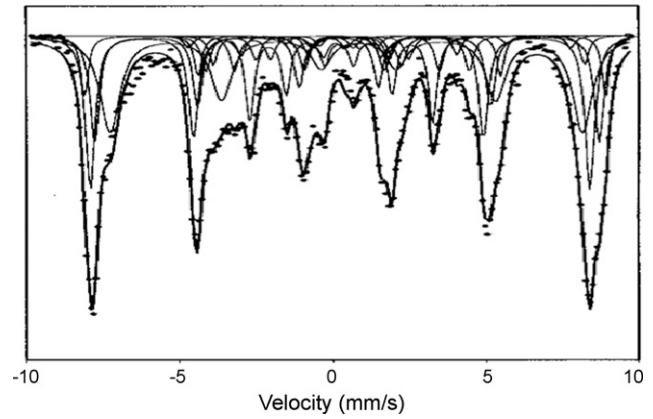

Fig. 4. Mössbauer spectrum at 20 K following H_2 activation and 143 h reaction time. (Fe_3O_4, 76%; χ-carbide, 8%; ε-carbide, 16%).

the Fe in the Magnetite form. In this case, both carbides, although low, remain stable or even increase slightly with reaction time, which resulted in a slight increase in CO conversion over the first 50 h of reaction time.

When both hydrogen and syngas was employed in activation, a low hydrogen partial pressure is required to minimize the water concentration in the reactor. When this is not the case the high water partial pressure can prevent Fe_3O_4 from being reduced further to form carbides [44]. Fig. 6 is the Mössbauer spectrum

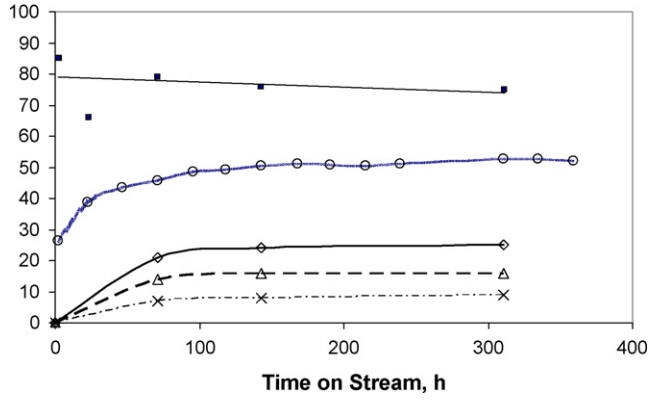

Fig. 5. CO conversion and iron carbide phases present during synthesis with a hydrogen activated iron catalyst (○, CO conversion; ■, Magnetite; △, ε-carbide; ×, χ-carbide; ◇, total carbides).

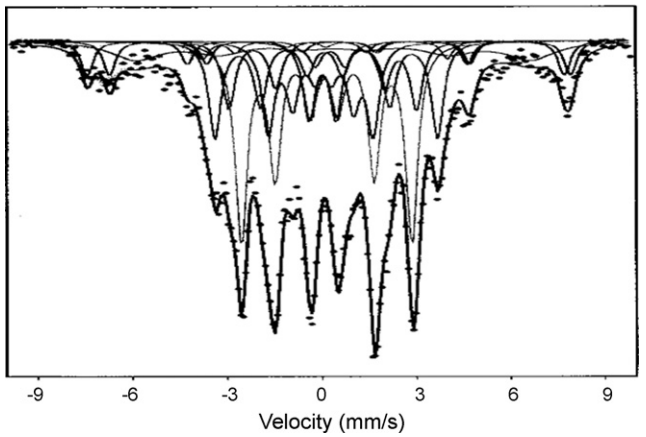

Fig. 6. Mössbauer spectrum at 20 K following syngas activation and 190 h reaction time. (Fe_3O_4, 21.5%; χ-carbide, 39.4%; ε-carbide, 33.3%; superparamagnetic, 5.8%).

obtained at 20 K from the syngas reduced iron catalyst after 190 h of FTS reaction time. Unlike the CO activated catalyst, the syngas activated iron catalyst contained a lower amount of χ-Fe_5C_2 than ε-$Fe_{2.2}C$. An initial ε-$Fe_{2.2}C$ as high as 64% was obtained at 24 h of reaction time, but it decreased gradually to below 30% while CO conversion decreased from 83% to 55% (Fig. 7). These data are in agreement with the results of Eliason and Bartholomew [44]. During the reaction period, χ-Fe_5C_2 increased from an initial 10% to 33%, which suggests that the conversion of ε-$Fe_{2.2}C$ to χ-Fe_5C_2 causes a deactivation of this iron catalyst. Magnetite changed little during the process; only the form of the carbides changed. The data in Table 3 show that the activation with syngas on the hydrocarbon rate is similar to that on CO conversion. The highest hydrocarbon rate was produced from the CO reduced catalyst (0.56 g/(h g-Iron)), which is slightly higher than that from syngas reduced catalyst, whereas hydrogen activation yielded a hydrocarbon rate as low as 0.34 g/(h g-Iron).

The activity of the syngas pretreated catalyst is similar to that of the CO pretreated sample (Fig. 7); however, it appears that the induction period is much shorter. The phases change significantly during the initial contact with syngas under the reaction conditions with Fe_3O_4 decreasing rapidly from about 60% to less than 20%. The initial carbide phase that is formed from Fe_3O_4 is ε-$Fe_{2.2}C$ which increases from about 30% to 60%, and then declines over the next 400 h to a stable level of about 30%. The χ-Fe_5C_2 phase increases from about 10% to 30% during the nearly 500 h run. The conversion shows little change during the significant initial

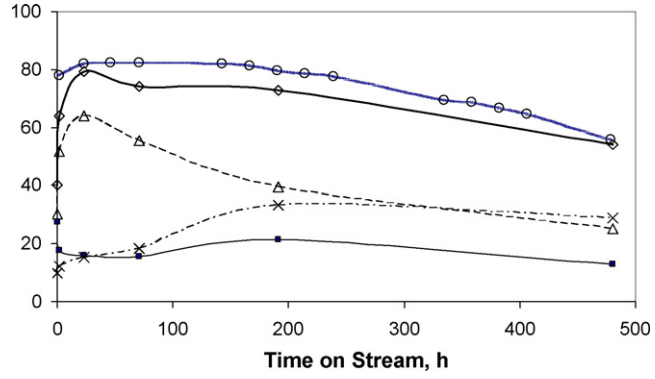

Fig. 7. CO conversion and iron carbide phase changes for a syngas activated iron catalyst (○, CO conversion; ■, Magnetite; △, ε-carbide; ×, χ-carbide; ◇, total carbides).

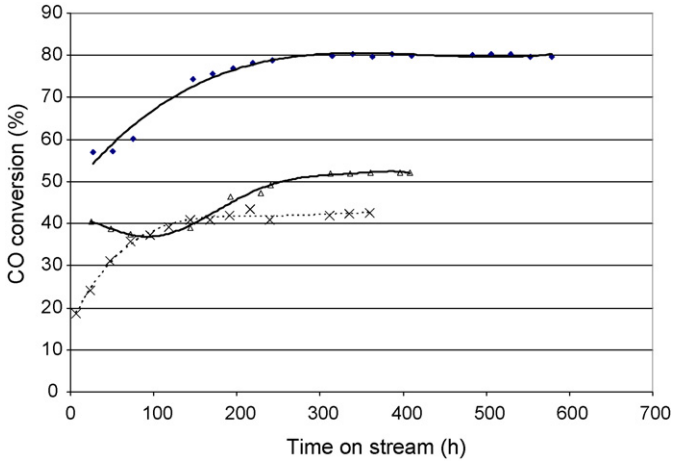

Fig. 8. Influence of activation gas on CO conversion following activation at 230 °C (◆, CO activation, 1.3 MPa; ×, hydrogen activation, 0.1 MPa; △, syngas activation, 0.1 MPa; FTS conditions: 270 °C, 1.3 MPa).

change in carbide phases, nor during the subsequent nearly 300 h of synthesis. From 200 to almost 500 h, the CO conversion slowly declines whereas the amounts of the two carbide phases remain essentially the same. Based upon the slow change in CO conversion while there is a major change in the ratio of the two carbide phases during the first 200 h of synthesis time, one would conclude that there is no direct relationship between the CO conversion and the bulk carbide phase as measured by Mössbauer spectroscopy.

3.2. Activation conditions

The catalyst was activated at three temperatures and then the activity/selectivity was determined at 270 °C. As shown in Fig. 8, for activation at 230 °C there was an induction period during the synthesis for each of the three pretreatments, with the CO and syngas pretreatments resulting in long induction periods. At this activation temperature, the CO pretreated sample had about 1.5 times the steady-state activity as that following the activation with H_2 or syngas. The trend of the results for the activation at 250 °C were similar to those obtained at 230 °C except that the induction period was shorter, with syngas activation an exception, and that the steady-state conversion was about 10% higher (Fig. 9). Likewise, a similar pattern was obtained following the activation

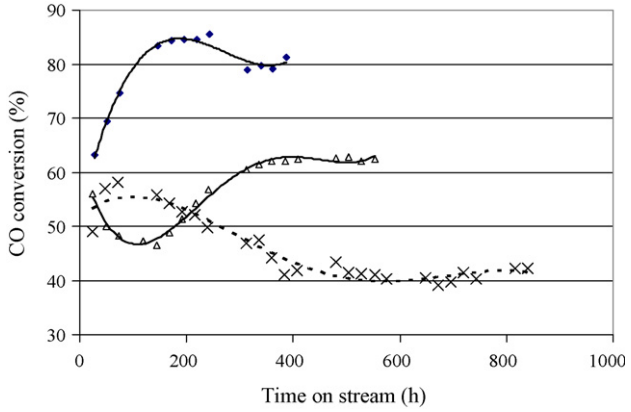

Fig. 9. Influence of activation gas on CO conversion following activation at 250 °C (◆, CO activation, 1.3 MPa; ×, hydrogen activation, 0.1 MPa; △, syngas activation, 0.1 MPa; FTS conditions: 270 °C, 1.3 MPa).

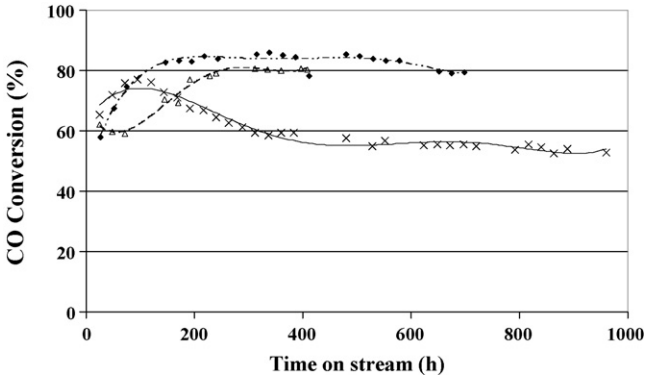

Fig. 10. Influence of activation gas on CO conversion following activation at 270 °C (◆, CO activation, 1.3 MPa; ×, hydrogen activation, 0.1 MPa; △, syngas activation, 0.1 MPa; FTS conditions: 270 °C, 1.3 MPa).

at 270 °C with the activity being about 10–20% higher CO conversion (Fig. 10). It appears that the induction period is the most prominent following activation at 270 °C.

The influence of the activation pressure with syngas was compared at the three temperatures for the catalyst. The conversion following activation at 1.3 MPa at the three temperatures was essentially the same and was lower than activation at atmospheric pressure (Fig. 11). The CO conversion following pretreatment increased with increasing activation temperature: from 40% to 60% to 80%.

3.3. Selectivity

The effect of activation gas on FTS alpha values are shown in Table 4. Although different reduction gases resulted in a significantly different catalytic activity, the alpha values for three activation gases were essentially the same. In all cases, an alpha value of 0.79–0.84 was obtained for α_1 and 0.90–0.92 for α_2. Similarly, different activation gases yielded similar hydrocarbon product distributions, as shown in Table 3.

Because olefins are more desired product in some applications due to their high reactivity, olefins are often employed in a chemical conversion process to produce other valuable chemicals. One advantage of an iron catalyst is the higher olefin selectivities than for the cobalt catalyst. Fig. 12 shows the olefin ratios in the

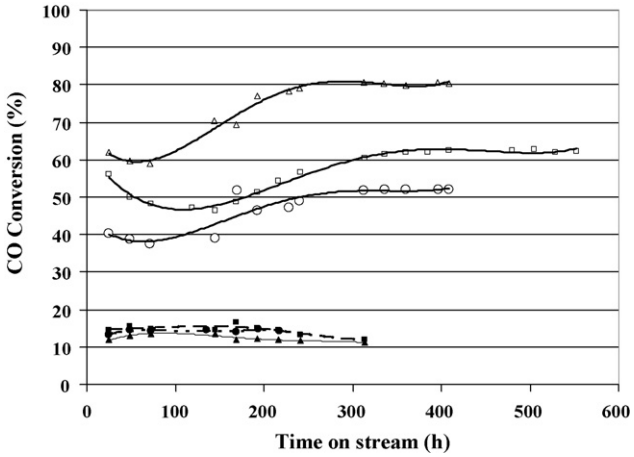

Fig. 11. Influence of pressure and temperature on CO conversion for syngas activation (●, syngas 230 °C, 1.3 MPa; ■, syngas 250 °C, 1.3 MPa; ▲, syngas 270 °C, 1.3 MPa; ○, syngas 230 °C, 0.1 MPa; □, syngas 250 °C, 0.1 MPa; △, syngas 270 °C, 0.1 MPa) (FTS conditions: 270 °C, 1.3 MPa).

Table 4
Alpha values for the catalyst following the three pretreatments.

Pretreatment gas	α_1[a]	α_2[a]
CO	0.84	0.92
H_2	0.79	0.89
Syngas	0.80	0.90

[a] Carbon numbers 1–33 used to calculate α_1 and 35–75 used to calculate α_2.

range of C_2–C_{20}. Starting from C_3, the olefin ratios decreased almost linearly from above 83% to below 20% for CO and syngas reduced catalysts. This is due to the secondary reactions in the CSTR. Both syngas and CO produced the same olefin ratios while H_2 yielded slightly higher olefin ratios, but at least some of this difference is due to the lower conversion. The low C_2 olefin ratio is due to its high activity for olefin readsorption reaction, as shown by ^{14}C tracer studies [53].

3.4. Water–gas shift

Water–gas shift is an important reaction in an FTS process when an iron catalyst is utilized. In this reaction, CO reacts with water, which is generated from FTS, and produces CO_2 and H_2. WGS produces the majority of the CO_2 for FTS, as given by Eq. (2). This WGS activity is an advantage of iron catalysts over the cobalt catalysts when low H_2/CO ratio syngas is used in an FTS reaction.

Some indicate that Magnetite and metallic iron [54–57] are more effective active sites for WGS than iron carbides. When an iron catalyst is used, water is adsorbed on the surface of the catalyst at an oxygen vacancy, and this results in the formation of hydrogen [1]. This process is then followed by the reduction step by CO, which removes oxygen in the form of CO_2 and regenerates the oxygen vacancy.

CO_2 selectivity can be used to compare the relative WGS activities for the three activations. The hydrocarbon selectivity ($1 - CO_2$ selectivity) results for the FTS reactions using three different activation gases are shown in Fig. 13. Both CO and H_2 activation generated slightly lower CO_2 selectivities than syngas activation. Although the stabilized CO_2 selectivities were similar among all three activation gases, H_2 activation produced lower initial CO_2 selectivity than CO reduction, while the latter was lower than syngas. This is in agreement with the results by some earlier work [2,58], suggesting that Magnetite is the active site for WGS reaction. The stabilized data in Fig. 13, however, cannot explain the similarity between differently reduced catalysts. As shown in Figs. 3, 5 and 7, after the induction period, Magnetite is at a level of about 40%, 75% and 20% for CO, H_2 and syngas reduced catalysts, respectively, but the CO_2 selectivity becomes essentially the same as indicated in Fig. 13. This is probably due to the surface changes that occur during the induction period. Unfortunately, the surface composition cannot be defined using the bulk structure measurements.

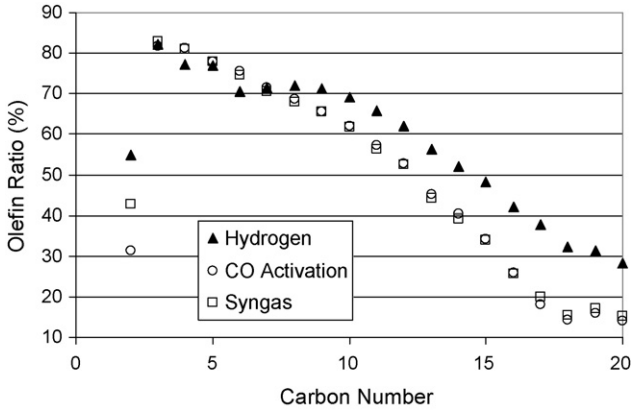

Fig. 12. Olefin ratios for increasing carbon number fractions following activation with CO, H_2 or syngas.

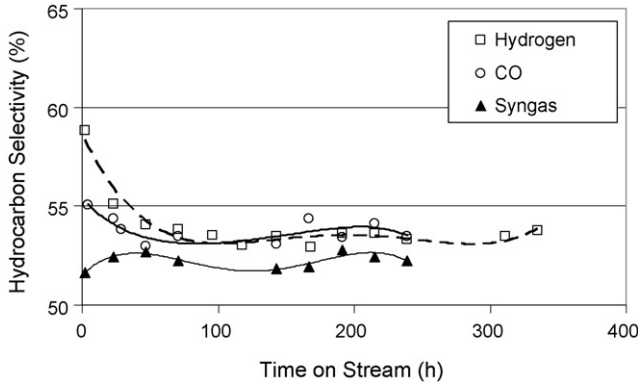

Fig. 13. Influence of activation gas on hydrocarbon selectivity for CO, H_2 and syngas activation.

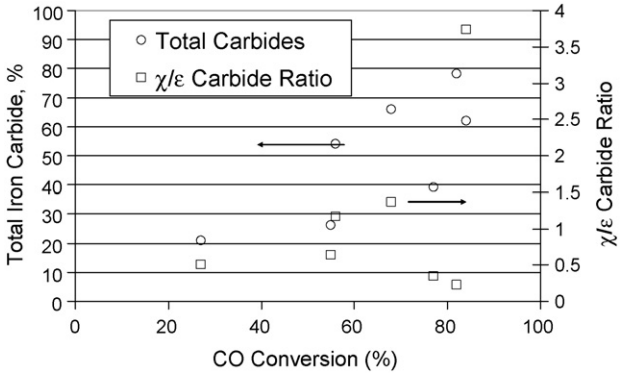

Fig. 14. χ/ε-iron carbide ratio versus CO conversion.

4. Conclusions

The pretreatment of a low alpha iron catalyst at atmospheric pressure with CO or syngas provides a higher activity than one pretreated with H_2. The product selectivity for the catalysts depended only slightly, if at all, on the pretreatment. The iron phases following pretreatment and during synthesis varied widely. It does not appear that the bulk iron phases determined by Mössbauer spectroscopy can be related directly to the catalyst activity (Fig. 14).

Acknowledgments

This work was supported by U.S. DOE contract number DE-FC26-98FT40308 and the Commonwealth of Kentucky.

References

[1] V.U.S. Rao, G.J. Steigel, G.J. Cinquegrane, R.D. Srivastava, Fuel Proc. Technol. 30 (1992) 83.
[2] D.B. Bukur, D. Mukesh, A.P. Snehal, Ind. Eng. Chem. Res. 29 (1990) 194.
[3] M.E. Dry, in: Bruce E. Leach (Ed.), Applied Industrial Catalysis, vol. 2, Academic Press, NY, 1983, p. 167.
[4] I.E. Wachs, D.J. Dwyer, E. Iglesia, Appl. Catal. 12 (1984) 201.

[5] C.D. Frohning, in: J. Falbe (Ed.), New Synthesis with Carbon Monoxide, Springer–Verlag, New York, 1980, p. 353.
[6] C. Li., Ph.D. Thesis, Texas A&M University, 1988.
[7] J.L. Rankins, C.H. Bartholomew, J. Catal. 100 (1986) 533.
[8] J.A. Dalmon, R. Dutartre, G.A. Martin, C. R. Acad. Sci. Ser. C 287 (1978) 557.
[9] D.J. Dwyer, J.H. Hardenburg, Appl. Surf. Sci. 19 (1984) 14.
[10] H.P. Bonzel, H.J. Kreb, Surf. Sci. 109 (1981) 1527.
[11] D.A. Wesner, F.P. Coenen, H.P. Bonzel, Langmuir 1 (1984) 478.
[12] M.E. Dry, Catal.: Sci. Technol. 1 (1981) 159–255.
[13] R.A. Dictor, A.T. Bell, J. Catal. 97 (1986) 121.
[14] R.J. O'Brien, L. Xu, R.L. Spicer, B.H. Davis, Symposium on syngas conversion to high value chemicals, in: Presented at the 211th ACS Annual Meeting, New Orleans, March 24–29, (1996), pp. 252–253.
[15] M.E. Dry, T. Shingles, L.J. Boshoff, G.J. Oosthuizen, J. Catal. 15 (1969) 190.
[16] J. Benziger, R.J. Madix, Surf. Sci. 94 (1980) 119.
[17] H. Arakawa, A.T. Bell, I & EC Proc. Des. Dev. 22 (1993) 97.
[18] M. Luo, B.H. Davis, Studies in Surface Science and Catalysis, vol. 139, Elsevier Science, 2001,, p. 133.
[19] R.B. Anderson, The Fischer-Tropsch Synthesis, Academic Press, New York, 1984.
[20] R.B. Anderson, Catalysis for Fischer-Tropsch Synthesis, in: P.H. Emmett (Ed.), Catalysis, vol. 4, Reinhold Publishing Corporation, New York, 1958, p. 29.
[21] M.D. Shroff, D.S. Kalakkad, K.E. Coulter, S.D. Kohler, M.S. Harrington, N.B. Jackson, A.G. Sault, A.K. Datye, J. Catal. 156 (1995) 185.
[22] A.J.H.M. Kock, H.M. Fortuin, J.W. Geus, J. Catal. 96 (1985) 261.
[23] X. Gao, J. Shen, Y. Hsia, Y. Chen, J. Chem. Soc. Faraday Trans. 89 (1993) 1079.
[24] Gmelins Handbuch der Anorganische Chemie, 59: Eisen, Teil A-Ableihung II, Verlag Chemie, Berlin, Germany, 1692.
[25] D.B. Bukur, L. Nowichi, X. Lang, Energy Fuels 9 (1995) 620.
[26] K.R.P.M. Rao, F.E. Huggins, V. Mahajan, G.P. Huffman, B.L. Rao, V.U.S. Bhatt, D.B. Bukur, B.H. Davis, R.J. O'Brien, Top. Catal. 2 (1995) 71.
[27] D.B. Bukur, M. Koranne, X. Lang, K.R.P.M. Rao, G.P. Huffman, Appl. Catal. A: Gen. 126 (1995) 85.
[28] J.P. Baltrus, J.R. Diehl, M.A. McDonald, M.F. Zarochak, Appl. Catal. 48 (1989) 199.
[29] K. Sudsakorn, J.G. Goodwin Jr., A.A. Adeyiga, J. Catal. 213 (2003) 204.
[30] A.G. Sault, J. Catal. 140 (1993) 121.
[31] E.S. Lox, G.B. Marin, E. De Graeve, P. Bussiere, Appl. Catal. A: Gen. 40 (1988) 197.
[32] R.J. O'Brien, Y. Zhang, H.H. Hamdeh, B.H. Davis, Preprints, 44(1) ACS, Div. Petr. Chem. Prepr. 44 (1999) 100.
[33] A.P. Raje, R.J. O'Brien, B.H. Davis, J. Catal. 180 (1998) 36.
[34] T. Komaya, A.T. Bell, J. Catal. 146 (1994) 237.
[35] G. Bian, A. Oonuki, N. Koizumi, H. Nomoto, M. Yamada, J. Mol. Catal. A: Chem. 186 (2002) 203.
[36] G.B. Raupp, W.N. Delgass, J. Catal. 58 (1979) 361.
[37] C.N. Satterfiled, R.T. Hanlon, S.E. Tung, Z. Zou, G.C. Papaefthymiou, Ind. Eng. Chem. Prod. Res. Dev. 25 (1986) 407.
[38] C.S. Huang, B. Ganguly, G.P. Huffman, F.E. Huggins, B.H. Davis, Fuel Sci. Technol. Int. 11 (1993) 1289.
[39] R.J. O'Brien, L. Xu, D.R. Milburn, Y.-X. Li, K.J. Klabunde, B.H. Davis, Top. Catal. 2 (1995) 1.
[40] R.J. O'Brien, L. Xu, R.L. Spicer, B.H. Davis, Energy Fuels 10 (1996) 921.
[41] K.R.P.M. Rao, F.E. Huggins, G.P. Huffman, R.J. Gormley, R.J. O'Brien, B.H. Davis, Energy Fuels 10 (1996) 546.
[42] G.L. Caer, J.M. Dubois, M. Pijolat, V. Perrichon, P. Bussiere, J. Phys. Chem. 86 (1982) 4799.
[43] J.A. Amelse, J.B. Butt, H. Schwartz, J. Phys. Chem. 82 (1978) 558.
[44] S.A. Eliason, C.H. Bartholomew, in: C.H. Bartholomew, G.A. Fuentes (Eds.), Catalyst Deactivation, Elsevier, 1997, pp. 517–526.
[45] J.A. Amelse, J.B. Butt, L.H. Schwartz, J. Phys. Chem. 82 (1978) 558.
[46] G.B. Raupp, W.N. Delgass, J. Catal. 58 (3 (July)) (1979) 348–360.
[47] H.H. Storch, N. Golumbic, R.B. Anderson, The Fischer-Tropsch and Related Syntheses, Wiley, 1951.
[48] J.P. Reymond, P. Mériaudeau, S.J. Teichner, J. Catal. 75 (1982) 39.
[49] M. Luo, B.H. Davis, Fuel Proc. Technol. 83 (2003) 49.
[50] M. Luo, R.J. O'Brien, S. Bao, B.H. Davis, Appl. Catal. A: Gen. 239 (2003) 111.
[51] M. Luo, B.H. Davis, Appl. Catal. A: Gen., to be submitted for publication.
[52] J.W. Niemantsverdriet, A.M. van der Kraan, W.L. van Dijk, H.S. van der Baan, J. Phys. Chem. 84 (1980) 3363.
[53] L.-M. Tau, H.A. Dabbagh, B.H. Davis, Energy Fuels 4 (1990) 94.
[54] R.J. Madon, S.C. Reyes, E. Iglesia, J. Phys. Chem. 95 (1991) 7795.
[55] R.J. Madon, E. Iglesia, J. Catal. 139 (1993) 576.
[56] E. Iglesia, S.C. Reyes, R.J. Madon, S.L. Soled, Adv. Catal. 39 (1993) 221.
[57] R.J. Madon, W.F. Taylor, J. Catal. 69 (1981) 32.
[58] B. Jagor, R. Espinoza, Catal. Today 23 (1995) 17.